Research Article | Vol. 9, No. 2 | 1 Feb 2018 | BIOMEDICAL OPTICS EXPRESS 569
Biomedical Optics EXPRESS

Diffuse optical monitoring of peripheral tissues during uncontrolled internal hemorrhage in a porcine model

KARTHIK VISHWANATH,[1,5,*] RAJAN GURJAR,[2,5] DAVID WOLF,[3,5] SUZANNAH RICCARDI,[2,5] MICHAEL DUGGAN,[4] AND DAVID KING[4]

[1]*Department of Physics, Miami University, Oxford, OH 45056, USA*
[2]*MIT Lincoln Laboratory, 244 Wood Street, Lexington, MA 02420, USA*
[3]*Warner Babcock Institute for Green Chemistry, 100 Research Drive, Wilmington, MA 01887, USA*
[4]*Division of Trauma, Emergency Surgery, and Surgical Critical Care, Massachusetts General Hospital, 165 Cambridge Street, Suite 810 Boston, MA 02114, USA*
[5]*Affiliations of authors when experiments were conducted: Radiation Monitoring Devices Inc., 44 Hunt Street, Watertown, MA 02472, USA*
**vishwak@miamioh.edu*

Abstract: Reliable, continuous and noninvasive blood flow and hemoglobin monitoring in trauma patients remains a critical, but generally unachieved goal. Two optical sensing methods - diffuse correlation spectroscopy (DCS) and diffuse reflectance spectroscopy (DRS) – are used to monitor and detect internal hemorrhage. Specifically, we investigate if cutaneous perfusion measurements acquired using DCS and DRS in peripheral (thighs and ear-lobe) tissues could detect severe hemorrhagic shock in a porcine model. Four animals underwent high-grade hepato-portal injury in a closed abdomen, to induce uncontrolled hemorrhage and were subsequently allowed to bleed for 10 minutes before fluid resuscitation. DRS and DCS measurements of cutaneous blood flow were acquired using fiber optical probes placed on the thigh and earlobe of the animals and were obtained repeatedly starting from 1 to 5 minutes pre-injury, up to several minutes post shock. Clear changes were observed in measured optical spectra across all animals at both sites. DCS-derived cutaneous blood flow decreased sharply during hemorrhage, while DRS-derived vascular saturation and hemoglobin paralleled cardiac output. All derived optical parameters had the steepest changes during the rapid initial hemorrhage unambiguously. This suggests that a combined DCS and DRS based device might provide an easy-to-use, non-invasive, internal-hemorrhage detection system that can be used across a wide array of clinical settings.

OCIS codes: (170.1610) Clinical applications; (170.6480) Spectroscopy, speckle; (170.6510) Spectroscopy, tissue diagnostics; (170.3660) Light propagation in tissues; (000.1430) Biology and medicine;

References and links

1. B. J. Eastridge, R. L. Mabry, P. Seguin, J. Cantrell, T. Tops, P. Uribe, O. Mallett, T. Zubko, L. Oetjen-Gerdes, T. E. Rasmussen, F. K. Butler, R. S. Kotwal, J. B. Holcomb, C. Wade, H. Champion, M. Lawnick, L. Moores, and L. H. Blackbourne, "Death on the battlefield (2001-2011): implications for the future of combat casualty care," J. Trauma Acute Care Surg. **73**(6 Suppl 5), S431–S437 (2012).
2. M. J. Joyner, "Orthostatic stress, haemorrhage and a bankrupt cardiovascular system," J. Physiol. **587**(21), 5015–5016 (2009).
3. D. S. Kauvar, R. Lefering, and C. E. Wade, "Impact of hemorrhage on trauma outcome: an overview of epidemiology, clinical presentations, and therapeutic considerations," J. Trauma **60**(6 Suppl), S3–S11 (2006).
4. M. J. Duggan, A. Y. Mejaddam, J. Beagle, M. A. Demoya, G. C. Velmahosa, H. B. Alam, A. Rago, G. Zugates, R. Busold, T. Freyman, U. Sharma, and D. R. King, "Development of a lethal, closed-abdomen grade V hepato-portal injury model in non-coagulopathic swine," J. Surg. Res. **182**(1), 101–107 (2013).
5. D. R. King, M. P. Ogilvie, B. M. Pereira, Y. Chang, R. J. Manning, J. A. Conner, C. I. Schulman, M. G. McKenney, and K. G. Proctor, "Heart rate variability as a triage tool in patients with trauma during prehospital helicopter transport," J. Trauma **67**(3), 436–440 (2009).
6. A. Y. Mejaddam, O. A. Birkhan, A. C. Sideris, G. M. Van der Wilden, A. M. Imam, J. O. Hwabejire, Y. Chang, G. C. Velmahos, P. J. Fagenholz, D. D. Yeh, M. A. de Moya, and D. R. King, "Real-time heart rate entropy

#309989 https://doi.org/10.1364/BOE.9.000569
Journal © 2018 Received 26 Oct 2017; revised 11 Dec 2017; accepted 22 Dec 2017; published 11 Jan 2018

Biomedical Optics EXPRESS

predicts the need for lifesaving interventions in trauma activation patients," J. Trauma Acute Care Surg. **75**(4), 607–612 (2013).
7. M. Duggan, A. Rago, U. Sharma, G. Zugates, T. Freyman, R. Busold, J. Caulkins, Q. Pham, Y. Chang, A. Mejaddam, J. Beagle, G. Velmahos, M. deMoya, L. Zukerberg, T. F. Ng, and L. T. C. D. R. King, "Self-expanding polyurethane polymer improves survival in a model of noncompressible massive abdominal hemorrhage," J. Trauma Acute Care Surg. **74**(6), 1462–1467 (2013).
8. M. P. Peev, A. Rago, J. O. Hwabejire, M. J. Duggan, J. Beagle, J. Marini, G. Zugates, R. Busold, T. Freyman, G. S. Velmahos, M. A. Demoya, D. D. Yeh, P. J. Fagenholz, U. Sharma, and D. R. King, "Self-expanding foam for prehospital treatment of severe intra-abdominal hemorrhage: dose finding study," J. Trauma Acute Care Surg. **76**(3), 619–624 (2014).
9. J. Q. Brown, K. Vishwanath, G. M. Palmer, and N. Ramanujam, "Advances in quantitative UV-visible spectroscopy for clinical and pre-clinical application in cancer," Curr. Opin. Biotechnol. **20**(1), 119–131 (2009).
10. M. C. Salcedo, K. Tart, and K. Hall, "A systematic review of human and veterinary applications of noninvasive tissue oxygen monitoring," J. Vet Emerg Crit Care **26**(3), 323–332 (2016).
11. A. Lima, "Current status of tissue monitoring in the management of shock," Curr. Opin. Crit. Care **22**(3), 274–278 (2016).
12. M. S. Green, S. Sehgal, and R. Tariq, "Near-Infrared Spectroscopy: The New Must Have Tool in the Intensive Care Unit?" Semin. Cardiothorac. Vasc. Anesth. **20**(3), 213–224 (2016).
13. M. Lipcsey, N. C. Woinarski, and R. Bellomo, "Near infrared spectroscopy (NIRS) of the thenar eminence in anesthesia and intensive care," Ann. Intensive Care **2**(1), 11 (2012).
14. G. Tachon, A. Harrois, S. Tanaka, H. Kato, O. Huet, J. Pottecher, E. Vicaut, and J. Duranteau, "Microcirculatory alterations in traumatic hemorrhagic shock," Crit. Care Med. **42**(6), 1433–1441 (2014).
15. J. H. Taylor, K. E. Mulier, D. E. Myers, and G. J. Beilman, "Use of near-infrared spectroscopy in early determination of irreversible hemorrhagic shock," J. Trauma **58**(6), 1119–1125 (2005).
16. T. Durduran and A. G. Yodh, "Diffuse correlation spectroscopy for non-invasive, micro-vascular cerebral blood flow measurement," Neuroimage **85**(Pt 1), 51–63 (2014).
17. Y. Shang, T. Li, and G. Yu, "Clinical applications of near-infrared diffuse correlation spectroscopy and tomography for tissue blood flow monitoring and imaging," Physiol. Meas. **38**(4), R1–R26 (2017).
18. T. Durduran, R. Choe, W. B. Baker, and A. G. Yodh, "Diffuse Optics for Tissue Monitoring and Tomography," Rep. Prog. Phys. **73**(7), 076701 (2010).
19. K. Vishwanath, R. Gurjar, S. Kuo, A. Fasi, R. Kim, S. Riccardi, S. E. Feinberg, and D. E. Wolf, "Sensing vascularization of ex-vivo produced oral mucosal equivalent (EVPOME) skin grafts in nude mice using optical spectroscopy," in *Photonic Therapeutics and Diagnostics* X. B. Choi, N. Kollias, H. Zeng, H. W. Kang, B. J. F. Wong, J. F. Ilgner, G. J. Tearney, K. W. Gregory, L. Marcu, and A. Mandelis, eds. (2014).
20. R. S. Gurjar, S. L. Riccardi, B. D. Johnson, C. P. Johnson, N. A. Paradis, M. J. Joyner, and D. E. Wolf, "Point-of-care optical tool to detect early stage of hemorrhage and shock," in *SPIE BiOS*(SPIE2014), p. 89510K.
21. K. Vishwanath, K. Chang, D. Klein, Y. F. Deng, V. Chang, J. E. Phelps, and N. Ramanujam, "Portable, Fiber-Based, Diffuse Reflection Spectroscopy (DRS) Systems for Estimating Tissue Optical Properties," Appl. Spectrosc. **65**(2), 206–215 (2011).
22. J. Malsan, R. Gurjar, D. Wolf, and K. Vishwanath, "Extracting optical properties of turbid media using radially and spectrally resolved diffuse reflectance," in *Design and Quality for Biomedical Technologies Vii*, R. Raghavachari, and R. Liang, eds. (2014).
23. G. M. Palmer and N. Ramanujam, "Monte Carlo-based inverse model for calculating tissue optical properties. Part I: Theory and validation on synthetic phantoms," Appl. Opt. **45**(5), 1062–1071 (2006).
24. M. Tivnan, R. Gurjar, D. E. Wolf, and K. Vishwanath, "High Frequency Sampling of TTL Pulses on a Raspberry Pi for Diffuse Correlation Spectroscopy Applications," Sensors (Basel) **15**(8), 19709–19722 (2015).
25. D. A. Boas and A. G. Yodh, "Spatially varying dynamical properties of turbid media probed with diffusing temporal light correlation," J. Opt. Soc. Am. A **14**(1), 192–215 (1997).
26. S. A. Carp, N. Roche-Labarbe, M. A. Franceschini, V. J. Srinivasan, S. Sakadžić, and D. A. Boas, "Due to intravascular multiple sequential scattering, Diffuse Correlation Spectroscopy of tissue primarily measures relative red blood cell motion within vessels," Biomed. Opt. Express **2**(7), 2047–2054 (2011).
27. V. V. Tuchin, S. R. Utz, and I. V. Yaroslavsky, "Tissue Optics, Light-Distribution, and Spectroscopy," Opt. Eng. **33**(10), 3178–3188 (1994).
28. A. Pifferi, P. Taroni, G. Valentini, and S. Andersson-Engels, "Real-time method for fitting time-resolved reflectance and transmittance measurements with a Monte Carlo model," Appl. Opt. **37**(13), 2774–2780 (1998).
29. M. K. Angele, C. P. Schneider, and I. H. Chaudry, "Bench-to-bedside review: latest results in hemorrhagic shock," Crit. Care **12**(4), 218 (2008).
30. B. Soller, C. Smith, F. Zou, G. E. Ellerby, M. D. Prince, and J. L. Sondeen, "Investigation of noninvasive muscle pH and oxygen saturation during uncontrolled hemorrhage and resuscitation in swine," Shock **42**(1), 44–51 (2014).
31. T. Kurita, K. Morita, and S. Sato, "The Influence of Hypovolemia and Fluid Resuscitation During Hemorrhagic Shock on Apneic Oxygen Desaturation After Preoxygenation in a Swine Model," Anesth. Analg. **121**(6), 1555–1561 (2015).
32. J. D. Sprick, B. R. Soller, and C. A. Rickards, "The efficacy of novel anatomical sites for the assessment of muscle oxygenation during central hypovolemia," Exp. Biol. Med. (Maywood) **241**(17), 2007–2013 (2016).

Biomedical Optics EXPRESS

33. C. Hinojosa-Laborde, R. E. Shade, G. W. Muniz, C. Bauer, K. A. Goei, H. F. Pidcoke, K. K. Chung, A. P. Cap, and V. A. Convertino, "Validation of lower body negative pressure as an experimental model of hemorrhage," J Appl Physiol (1985) **116**, 406– 415 (2014).
34. K. R. Ward, M. H. Tiba, K. L. Ryan, I. P. Filho, C. A. Rickards, T. Witten, B. R. Soller, D. A. Ludwig, and V. A. Convertino, "Oxygen transport characterization of a human model of progressive hemorrhage," Resuscitation **81**(8), 987–993 (2010).
35. V. Jain, E. M. Buckley, D. J. Licht, J. M. Lynch, P. J. Schwab, M. Y. Naim, N. A. Lavin, S. C. Nicolson, L. M. Montenegro, A. G. Yodh, and F. W. Wehrli, "Cerebral oxygen metabolism in neonates with congenital heart disease quantified by MRI and optics," J. Cereb. Blood Flow Metab. **34**(3), 380–388 (2014).
36. M. N. Kim, T. Durduran, S. Frangos, B. L. Edlow, E. M. Buckley, H. E. Moss, C. Zhou, G. Yu, R. Choe, E. Maloney-Wilensky, R. L. Wolf, M. S. Grady, J. H. Greenberg, J. M. Levine, A. G. Yodh, J. A. Detre, and W. A. Kofke, "Noninvasive measurement of cerebral blood flow and blood oxygenation using near-infrared and diffuse correlation spectroscopies in critically brain-injured adults," Neurocrit. Care **12**(2), 173–180 (2010).
37. R. Schlichtig, D. J. Kramer, and M. R. Pinsky, "Flow redistribution during progressive hemorrhage is a determinant of critical O_2 delivery," J. Appl. Physiol. **70**(1), 169–178 (1991).
38. A. Tripathi and E. R. Nadel, "Forearm skin and muscle vasoconstriction during lower body negative pressure," J Appl Physiol (1985) **60**, 1535– 1541 (1986).
39. P. Wellhöner, D. Rolle, P. Lönnroth, L. Strindberg, M. Elam, and C. Dodt, "Laser-Doppler flowmetry reveals rapid perfusion changes in adipose tissue of lean and obese females," Am. J. Physiol. Endocrinol. Metab. **291**(5), E1025–E1030 (2006).
40. R. M. Brothers, J. E. Wingo, K. A. Hubing, and C. G. Crandall, "Methodological assessment of skin and limb blood flows in the human forearm during thermal and baroreceptor provocations," J Appl Physiol (1985) **109**, 895– 900 (2010).
41. D. Gagnon, R. Matthew Brothers, M. S. Ganio, J. L. Hastings, and C. G. Crandall, "Forehead versus forearm skin vascular responses at presyncope in humans," Am. J. Physiol. Regul. Integr. Comp. Physiol. **307**(7), R908–R913 (2014).
42. K. R. Ward, R. R. Ivatury, R. W. Barbee, J. Terner, R. Pittman, I. P. Filho, and B. Spiess, "Near infrared spectroscopy for evaluation of the trauma patient: a technology review," Resuscitation **68**(1), 27–44 (2006).

1. Introduction

There is an unmet need to non-invasively detect and monitor internal bleeding caused by trauma in civilians and warfighters. Injury can result in occult hemorrhage and severe shock, which if not diagnosed and treated early, can result in significant morbidity or death [1–3]. When detected early, interventions can dramatically reduce the mortality rate of hemorrhage. Noninvasive measures that can detect hemorrhage and shock may be useful, particularly in the prehospital or battlefield environment, when standard measures of shock (such as blood pressure) are unreliable, difficult to obtain, or simply not available.

In response to hemorrhage, blood from the skin and extremities is shunted by vascular constriction to maintain perfusion to vital organs such as brain and kidneys [4–6]. Additionally, standard physiological indicators such as blood pressure and heart rate are not reliable indicators of severe bleeding until all physiologic reserve has been exhausted [7, 8]. An ideal indicator of hemorrhage would be expected to correlate with blood loss, while also possessing a large dynamic range such that subtle changes in homeostasis during early stages of hemorrhage are resolved. Further, these indicators of hemorrhage should be noninvasive, continuous, and not require significant operator skills (such as a standard sphygmomanometer).

Near infrared or visible diffuse reflectance spectroscopy (DRS) is a spectroscopic technique that non-invasively captures the diffusely reflected spectrum from a (tissue) surface of interest and allows extraction of tissue hemoglobin concentration and oxygenation [9]. Both these hemodynamic parameters obtained via DRS methods have been widely explored to monitor shock and have previously been well-reviewed [10–15].

Although, tissue hemoglobin saturation and concentration are important physiological markers that are impacted by shock, peripheral tissue microcirculation would also be significantly impacted and could provide additional information to detect shock. Diffuse correlation spectroscopy (DCS) is a laser light scattering technique method that has been developed to characterize (micro)vascular flow and has been used to monitor tissue blood flow across several different studies [16–18].

Biomedical Optics EXPRESS

Towards that end, we present a pilot study that used two optical methods – DCS and DRS – that were used together to continuously monitor tissue hemodynamics in a swine model of hemorrhagic shock. It was hypothesized that noninvasive measurements of DCS (to detect microvascular blood flow) and DRS (to detect tissue hemoglobin concentration and saturation) within peripheral tissues would capture systemic physiological changes during uncontrolled hemorrhage.

2. Methods

2.1 Animal study protocol

The study was approved by the Institutional Animal Care and Use Committee of Massachusetts General Hospital. Female Yorkshire swine, 38-48 kg, were utilized following a period of cage adjustment and a 12 hour pre-operative solid-food fast. Following induction of general anesthesia, all animals were invasively instrumented and monitored according to previously described methods [4, 7, 8]. Animals underwent Swan-Ganz thermodilution pulmonary artery catheter placement and arterial monitoring via cut-down in the neck. The liver was instrumented at laparotomy with percutaneous cutting wires, such that distraction of the wires (after laparotomy closure) resulted in severe, uncontrolled hemorrhage in the hepatic and portal vein and sudden, massive hypotension. Lactated Ringer's resuscitation was initiated ten minutes after injury and animals were resuscitated to a goal mean arterial pressure (MAP) of 65 mmHg. A time-series of optical DCS and DRS were made on opposite thighs from N = 4 animals. Optical measurements for each animal spanned time points from baseline (pre-injury) through recovery. Figure 1 shows images of the optical probes placed on an animal prior to start of the experiment. A second DCS measurement was also made across the animal's ear (in transmission mode, and is shown in Fig. 1(b)). The locations of probe peripheral sites were chosen, mainly, regarding practical convenience for experimental access during the surgical protocol.

2.2 Instrumentation and data acquisition

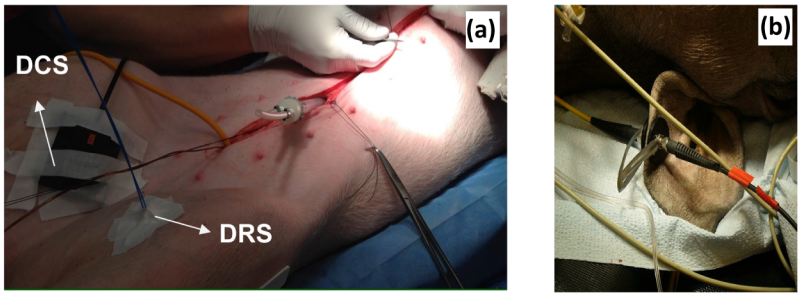

Fig. 1. Images of the animal preparation along with optical probes. Figure 1(a) shows the probes on the thighs of the animal while Fig. 1(b) shows the ear (transmission) DCS probe.

2.2.1 DCS

Fiberoptic-based DCS measurements were obtained using a custom-built instrument described previously [19, 20]. Two narrow linewidth (<0.02nm, coherence length > 5m) power stabilized 50mW laser diodes, operating at 785 nm (Thornaby Inc., Newton, NJ used for the ear-channel and Innovative Photonics, Monmouth Junction, NJ used for the reflectance channels) were each coupled to two 200 µm optical fibers that delivered nearly 1mW of power to tissue sites of interest. Diffusely reflected and transmitted optical signal were detected by three, separate, 10 µm diameter optical fibers (two in reflection mode and one in transmission). Although there were two different laser sources used, their coherence properties were similar and provided reliable signals across all DCS channels. In the

Biomedical Optics EXPRESS

reflection mode, the center-center distances for the source-detection fiber-pairs were 0.2 cm and 1cm, while the diffusely scattered transmission was recorded across the earlobe via single input and output fibers (See 1A and 1B). The detection fibers were each coupled to three separate single photon-counting modules - the two reflection probes to the ID120 (ID Quantique, Geneva, Switzerland and the transmission channel to an SPCM-AQRH (Excelitas Tech. Corp., Waltham, MA). Outputs from each were fed into an 8-channel digital autocorrelator (Flex05-8ch, Correlator.com) to calculate intensity autocorrelation functions ($g_2(\tau)$).

Data were collected sequentially – from 0.2 cm channel first, the 1 cm channel next, and last from the transmission probe. For each animal, the DCS instrumentation was set up as the animal was being prepared for the surgery and baseline measurements were started as soon as the animal was anesthetized. Each DCS correlation per channel lasted nearly 4 seconds and thus, a complete set of DCS scans were obtained nearly every 12 s. Longitudinal scans were manually triggered and obtained for each animal for total durations ranging from 5 to 20 minutes of baseline and till resuscitation was initiated. More than 150 DCS scans were obtained per animal (from start to resuscitation).

2.2.2 DRS

A single-channel, portable, fiber-optical diffuse reflectance spectroscopy system described previously was used to acquire DRS measurements [21]. Light from a Halogen lamp (HL2000, Ocean Optics, Dunedain, FL) was coupled to one end of a custom-built bifurcated fiber probe containing two 600 μm diameter optical fibers. Light was delivered to the tissue surface using one of these fibers and the diffuse reflectance from the thigh was collected by a second identical optical fiber that was placed 2.6 mm from the source fiber. The detected light was coupled to a spectrometer (USB4000, Ocean Optics, Dunedain, FL) to record the diffuse reflectance from the tissue. (See Fig. 1(a) for the placement of the DRS fiber probe on a representative animal). Along with collection of tissue reflectance signals, reflectance data were acquired (at the beginning and the end of each animal run) from a 99% white spectralon reflectance standard (Labsphere, North Sutton, NH, USA) and from a calibrated, homogenous solid tissue phantom block (INO, Hamilton, Ontario, Canada).

Like the DCS measurements, DRS reflectance scans were collected longitudinally for each animal, beginning with animal anesthetization. Each DRS scan required an integration time of 100 ms and longitudinal scans were manually triggered and obtained from each animal for total durations ranging from 35 to 90 minutes. More than 230 DRS scans were obtained per animal (from baseline to resuscitation).

2.3 Data analysis

2.3.1 DRS

The collected diffuse reflectance spectra were stored and subsequently analyzed using a Monte Carlo based inverse model over a spectral region spanning 480-800 nm as described previously [22]. Briefly, each measured spectrum was background corrected for dark noise correction and normalized by 99% reflectance standard. This normalized diffuse reflectance spectrum, together with the normalized reflectance measurement from the reference phantom was input into the inverse Monte Carlo to generate a model-predicted, calibrated diffuse reflectance spectrum (see Fig. 2(b) for representative measured and fit data). The parameters for fitting included the *A* and *b* coefficients to model the reduced scattering coefficient of the medium: $\mu'_s(\lambda) = A\lambda^{-b}$ and the concentrations of the oxy- and deoxy-hemoglobin concentrations, [HbO_2] and [dHb], respectively, in the tissue volume probed as detailed previously elsewhere [21, 23]. These concentrations were summed to yield the total hemoglobin concentration ([THb] = [HbO_2] + [dHb]) and the vascular saturation (100 × [HbO_2]/ [THb]).

Biomedical Optics EXPRESS

2.3.2 DCS

Since our DCS measurements included data that were obtained in the transmission mode (Ear channel) as well as short-source detector reflection geometry (0.2 cm channel), the DCS data were analyzed using two different techniques.

The first method was heuristically developed and sought to associate a $\tau_{0.5}$ value for each measured intensity autocorrelation [24]. The $\tau_{0.5}$ value provides a unit of time characterizing the correlation time when $g_2(\tau)$ had decayed to half the difference of the mean value of $g_2(\tau)$ during early intervals (10^{-6}-10^{-5} s) and late intervals (1-2 s). (See Fig. 2(a) for a schematic illustration). The reciprocal of the $\tau_{0.5}$ value was used to represent a flow-index (in AU) and represents a simple scalar factor to quantify the decay of a given autocorrelation trace. Thus, DCS scans (for each channel and each measurement point) were translated into a corresponding $1/\tau_{0.5}$ flow-index value. This method was empirical in nature and only required experimental data to derive the flow-index.

The second method was a theoretical fit of the intensity autocorrelation using the well-established diffusion theory based expression for the unnormalized field correlation measured using reflectance geometry from a semi-infinite medium [25]. This closed-form expression included dependence on both the tissue optical absorption and scattering coefficients and on the movement of scatterers, which was set to be of the Brownian form here [16]. The fitting process yielded an effective flow parameter, which is expressed here as αD_B, following same notations used previously [16, 26]. Although all three DCS channels were modeled using the same analytical expression, the theory is only expected to be valid for measurements obtained from the 1cm channel (since data for the 0.2 cm source-detector geometry may not be accurately modeled via diffusion theory and the semi-infinite model of reflectance has different functional form transmission through thin-slab [27, 28]). Additionally, the data for all DCS scans (for each channel) were fit to tissue absorption and scattering coefficients obtained from DRS that were matched in time to the closest DCS scans.

2.3.3 Time synchronization between DCS and DRS

Since the DCS and DRS signals were collected on separate machines and involved two independent operators, a relative time-scale was constructed using the time-stamps of the stored data on each machine in seconds. On this scale, each animal is adjusted so that the

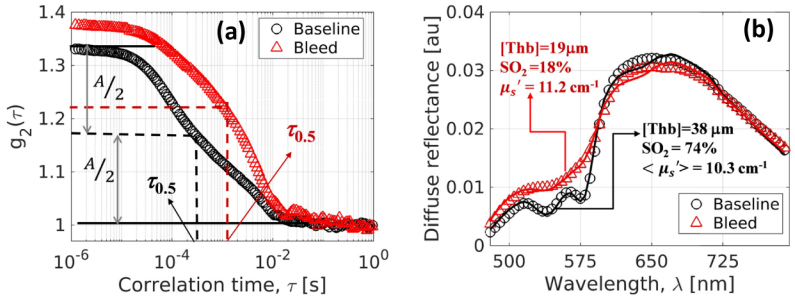

Fig. 2. Representative DCS signal measured for the ear channel (Fig. 2(a)) and DRS spectra (Fig. 2(b)) acquired before injury (black curves - baseline) and 100s post injury (red curves - bleed) for one animal. Figure 2(a) illustrates how $\tau_{0.5}$ (see text) was computed for each trace. Figure 2(b) shows the corrected DRS spectra measured in the same animal, at nearly the same times as the DCS curves (symbols) and the corresponding MC fits (lines).

injury point is marked as $t = 0$. This process naturally induced some uncertainty in marking exact timing of each acquisition for comparisons between DRS and DCS data. Given that experimental DCS scans for all channels were recorded every 12 s, while the sampling rate of

Biomedical Optics EXPRESS

the DRS scans were manually triggered at 0.5-2 Hz, we estimated that we this uncertainty to ≤ 2 s.

3. Results

3.1 Representative DCS and DRS measurements and parametrizations

Figure 2 shows the measured DCS (Fig. 2(a)) and DRS (Fig. 2(b)) signals from one representative animal acquired at two different times – at baseline (blue) and during bleed (red). The data in Fig. 2(a) are shown for the ear transmission DCS channel and show that the measured $g_2(\tau)$ decays more slowly, or with increased $\tau_{0.5}$ (or a reduced flow index), commensurate with the physiological status of the animal under these two conditions. The indicated$\tau_{0.5}$ values for these data differ by over an order of magnitude. Figure 2(b) shows the

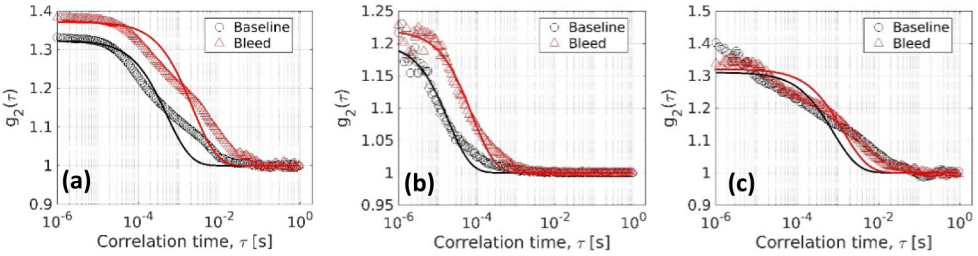

Fig. 3. Representative DCS signal measured for the ear transmittance channel (Fig. 3(a)), the 1 cm reflectance channel (Fig. 3(b)) and the 0.2 cm channel (Fig. 3(c)). The two traces show points of baseline (in black) and bleed (in red) for the same times and animal as Fig. 2. The solid line shows the diffusion theory based fits.

corrected reflectance spectra acquired using DRS for the same animal at nearly the same times as the DCS traces. The symbols show the measured data and the lines indicate the inverse Monte Carlo model-based fitting. The derived vascular saturation (SO_2), total hemoglobin concentration ([THb]) and the mean scattering coefficient ($<\mu_s'>$) from these data are noted in Fig. 2(b) and were as anticipated for conditions of rapid uncontrolled bleed relative to baseline.

Figure 3(a)-3(c) show measured DCS data (symbols) for the same animal, at the same two times as in Fig. 2 across all the three channels along with the diffusion theory based fits (solid lines). Measured data in Fig. 3(a) is the same as Fig. 2(a) (ear channel), while Fig. 3(b) and Fig. 3(c) show these data recorded for 1cm and 0.2cm reflectance channels, respectively. As expected the diffusion theory fits experimental data best for the 1cm channel (Fig. 3(b)). Both the ear channel and 0.2 cm reflectance channel data (Fig. 3(a) and 3(c)) show that although the diffusion theory does not fit the data as well as the 1cm channel, the extracted fits did capture slower decays of the autocorrelation traces measured during bleed. Interestingly, theoretical fits to the transmission mode measurements appeared to have lower residuals relative to the diffusion theory fits for the 0.2 cm channel.

3.2 Measured time-course in derived optical parameters

Figure 4 shows normalized time-courses in blood-flow index values derived from DCS using both analytical strategies – Fig. 4(a)-4(c) show these data for the flow-index derived using $1/\tau_{0.5}$, while Fig. 4(d)-4(f) show the derived flow-index αD_B, obtained from diffusion theory fits. The data for each animal in these figures were normalized such that the flow-index from the last measurement prior to injury was set to unity (and denotes the fraction-change in the flow indices, relative to this point). The data for the ear transmission channel, the 1cm channel and the 0.2 cm channel are plotted in Fig. 4(a) and Fig. 4(d), Fig. 4(b) and Fig. 4(e),

Biomedical Optics EXPRESS

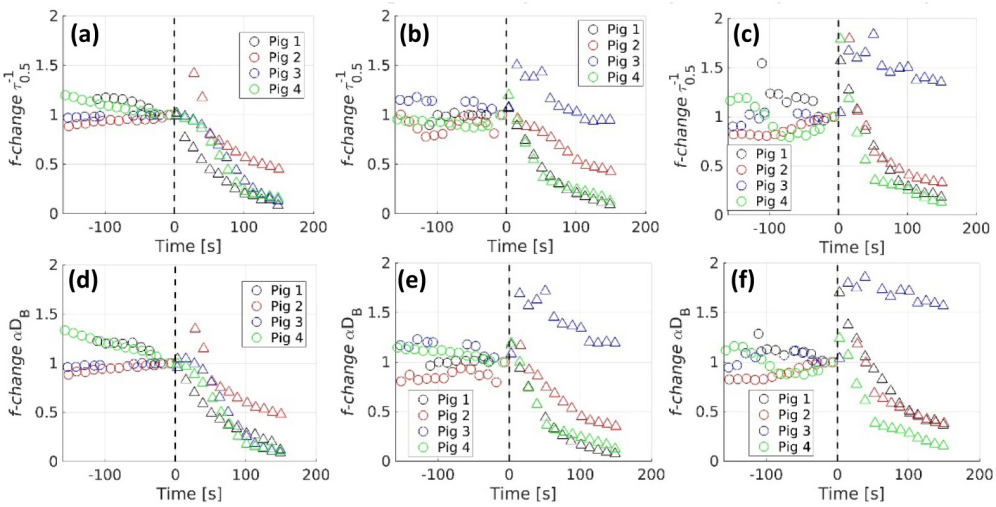

Fig. 4. Normalized longitudinal variations in flow index derived from DCS using both analytical strategies (see text). Symbols differentiate pre-injury (baseline: circles) from post-injury (bleed: triangles), while each color corresponds to a different animal. The vertical line at $t = 0$ indicates time of induced hemorrhage. Data in Fig. 4(a) and 4(d) are for the ear channel, for 4(b) and (e) are for the 1cm reflectance channel and 4(c) and 4(f) for the 0.2 cm reflectance channel, respectively.

and Fig. 4(c) and Fig. 4(f), respectively. Data acquired pre-injury (baseline) and post-injury (bleed) are shown as different symbols (circles: baseline; triangles: bleed) while different colors correspond to animals. These data indicate that the DCS-derived flow-index in all animals decreased from baseline to bleed as anticipated. It is also evident that the responses were different for each channel. Overall, the transmission ear channel was most sensitive to bleed and showed changes within seconds post-injury in all animals. It is remarkable that the data obtained using two completely different analytical strategies (flow index as $1/\tau_{0.5}$ and as

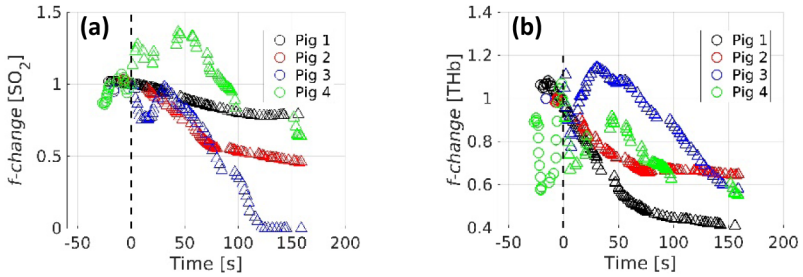

Fig. 5. Longitudinal changes in normalized SO_2 (Fig. 5(a)) and [THb] (Fig. 5(b)) derived from DRS for each animal. Symbols mark pre-injury (baseline: circles) and post-injury (bleed: triangles), while each color corresponds to a different animal. The vertical line at $t = 0$ indicates time of induced hemorrhage.

αD_B) appear as similar as shown Fig. 4, thus indicating that either of these two methods provide equivalent information about the underlying flow as was noted previously [24].

Figure 5 shows normalized time-trends obtained for the DRS-derived optical variables (Fig. 5(a): SO_2 and Fig. 5(b): [THb]) where, as before, the scan prior to injury was set to unity. These are shown with the same symbols and colors as Fig. 4 (circles: baseline; triangles: bleed) with different colors corresponding to different animals. These data show that DRS variables underwent expected changes for these hemodynamic variables with bleed, but the latency of changes in these variables was different from those seen for the DCS data,

Biomedical Optics EXPRESS

especially in Pigs 3 and 4. The DRS variables also exhibited larger degree of heterogeneity in the temporal course of responses, across animals.

3.3 Mean responses of DCS and DRS variables to uncontrolled hemorrhage

These normalized, diffusion theory based flow-index variable (αD_B) were averaged across all

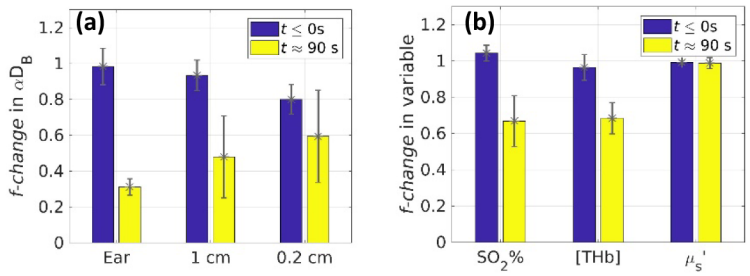

Fig. 6. Mean fractional change in flow index from diffusion theory fits (Fig. 6(a)) and DRS variables (Fig. 6(b)) across all four animals. Bars are average values obtained in each animal during baseline while the bleed values were obtained at 90s post injury. Whiskers indicate standard deviations.

animals to determine the fractional changes in the flow-index 90s post injury relative to the baseline values, in each DCS channel and are shown in Fig. 6(a). The baseline values for each animal were obtained as the mean fractional change (shown in Fig. 4(d)) for all times before injury while the 90s value was obtained from the scan at nearly 90s post injury. The mean fractional decrease in the flow-index derived for the ear channel showed the largest decrease during at 90s past injury (the flow-index decreases by nearly 80% of its value at baseline). The 1cm channel showed the next largest decreases (of 51%) with the 0.2cm channel showing decreases of 40%. These data also indicate that the responses across all animals were most consistent in the transmission channel (ear) and least for the 0.2cm reflectance channel.

Figure 6(b) shows the normalized changes for the DRS derived variables of vascular saturation (SO_2%), total hemoglobin concentration ([THb]) and the wavelength averaged reduced scattering ($<\mu_s'>$). Both the hemodynamic variables showed decreases of 30-40% between baseline and bleed conditions while the scattering remained largely unchanged. In comparison with the data in Fig. 6(a), the DRS derived variables showed lower decreases than the DCS-derived fractional change in flow rates.

3.4 Relationships of optical variables and systemic clinical indicators of shock

Table 1 lists systemic clinical parameters that were monitored across the four animals used in these experiments. The data here were obtained from the clinical instrumentation placed in these animals, post anesthesia and included measurements of heart rate (HR), mean arterial pressure (MAP), cardiac output (CO), cutaneous arterial saturation (SpO2) and core body temperature (Temp.). These parameters were recorded in 5-minute intervals. Thus, data from start of experiment to injury (for nearly 20-30 minutes for each animal) were used to compute as pre-injury estimates, while data for 15 minutes following shock was used to calculate the post-bleed values shown Table 1. Overall, all animals showed reductions in cardiac output, mean arterial pressure, temperature and arterial saturation post-injury, relative to baseline values. MAP and CO variables showed consistent decreases for each animal while SpO_2 did not decrease uniformly in all animals.

A direct temporal comparison for changes in these clinical variables and the optical hemodynamic variables measured was not possible since the optical data was sampled at far higher acquisition rates, relative to the clinical data. We did compare the mean clinical

Biomedical Optics EXPRESS

variables shown for each animal in Table 1 with corresponding optical variables measured for baseline or the bleed intervals but did not find significant correlations in them. However, in comparing the fractional changes in DCS-derived flow with changes in these clinical variables, we found it was positively (not significantly) associated with the change in MAP and negatively associated to with change in CO, for all the three channels used. These trends were mirrored by the DRS-derived [THb] and but absent for the DRS-derived SO_2.

4. Discussion

Table 1. Systemic variables at baseline (pre) and following shock (post) for the 4 animals. Data for each variable are shown as the mean value with standard deviations in parentheses. The last column presents the averages for these data across all animals.

Clinical variable	Pig1		Pig2		Pig3		Pig4		*Average*	
	Pre	***Post***	***Pre***	***Post***	***Pre***	***Post***	***Pre***	***Post***	***Pre***	***Post***
HR (bpm)	90.0 (3.0)	119.5 (27.5)	82.9 (3.8)	136.8 (37.4)	90.9 (5.6)	134.5 (61.3)	101.1 (3.0)	152.5 (41.3)	91.2 (8.3)	130.9 (86.9)
MAP (mmHg)	65.7 (5.6)	36.5 (19)	68.0 (5.7)	35.3 (17.5)	58.3 (7.4)	34.0 (17.6)	82.4 (14.5)	36.5 (13.8)	68.6 (18.1)	35.6 (34.1)
CO (L/min)	5.3 (0.3)	4.1 (1.9)	4.9 (0.4)	2.9 (1.5)	6.0 (0.3)	4.2 (2.3)	5.6 (0.5)	3.9 (2.4)	5.5 (0.8)	3.8 (4.1)
SpO_2 (%)	98.0 (0.2)	98.5 (0.7)	96.1 (1.6)	88.0 (1.4)	95.7 (1.1)	93.3 (6.2)	98.6 (0.5)	97.7 (0.6)	97.1 (1.9)	94.4 (6.4)
Temp. (°C)	36.0 (0.2)	35.5 (0.2)	36.2 (0.2)	35.8 (0.3)	37.3 (0.2)	36.7 (0.3)	36.9 (0.1)	36.4 (0.1)	36.6 (0.3)	36.1 (0.5)

An essential component of the reflex compensatory response to blood loss is constriction of the blood vessels within peripheral tissue beds to maintain perfusion of the brain and heart [29]. The shallowest (smallest) vessels in microvasculature is where compensatory blood shunting occurs and thus would comprise of the first vessels to be affected due to vasoconstriction following shock along with the last vessels to recover during resuscitation. Several groups have shown that monitoring of peripheral tissue perfusion and oxygenation provides an early indication of progressive hemorrhage (or experimental central hypovolemia), before full circulatory collapse occurs [20, 30–32].

This reduction in cutaneous perfusion can be expected to manifest in three parameters in the following temporal order: 1) Slowing of flow rate (decrease in DCS-derived flow-index) 2) reduction of the amount of blood in the tissue (DRS-derived [THb]), and 3) decrease in tissue oxygenation level (DRS-derived SO_2). As hemorrhage progresses, THb and SO_2 may expected to reduce further, since total blood volume decreases due to bleed and hematocrit decreases because of dilution with interstitial fluid. Our study indicates that noninvasive optical measurements based on DCS and DRS can be used to simultaneously detect this cascade of cutaneous, perfusion reducing events.

Earlier results obtained using DCS to monitor hemorrhage in a slow bleed pig model and in the lower body negative pressure model (LBNP) also support findings here [20]. In these previous studies, sensitivity of DCS measurement to changes occur early during compensatory hemorrhage was observed. However, the hemorrhage models used there were deficient in that they were highly clinically controlled and might not potentially not include inflammatory elements of immune response associated with soft tissue injury, or closed fractures that invariably accompany traumatic injuries particularly under military conditions. Additionally, two recent critical comparisons of hemorrhage and LBNP, one in baboons [33] the other in humans [34], have shown that the LBNP model effectively models the hemodynamic aspects of hemorrhage, such as heart rate stroke volume, and MAP, but not essential oxygen transport aspects, such as the reduction of $SmvO_2$.

Other techniques using acoustic and/or electrical sensing have been described to monitor hemorrhage but have also noted to be slow to respond, or respond weakly [8, 35–37]. The most direct comparisons may be made between DCS and Laser Doppler Flowmetry (LDF). Several studies have reported using LDF to monitor hemorrhage in porcine and the human

Biomedical Optics EXPRESS

lower body negative pressure (LBNP) models [38–41] and in general support the prospect of detecting capillary flow to monitor the early onset of hemorrhage. The results nevertheless, especially with LBNP, are equivocal –with some reports observing some of these effects and others missing them.

In general, however, results with LBNP studies observed smaller magnitude of than detected using DCS. While both LDF and DCS measure the fluctuations in the laser speckle pattern generated by blood cell movement, LDF detects these fluctuations in the frequency domain, while DCS performs it in the time domain. Typically, frequency domain measurements require uniform spacing of the frequencies, while in DCS analysis is intrinsically a logarithmic process. This difference confines LDF measurements to have dynamic range of about three orders, while in DCS measurements covers dynamic range of seven to ten orders of magnitude (from 100 ns −10 s). Although DCS can monitor very high frequency (short time) events, it is still an intrinsically time-integrated technique. The detected autocorrelation function is continuously accumulated and binned into multiple orders of magnitude which renders the method slow for data acquisition, but provides higher signal-to-noise advantage over LDF.

DRS has extensively been used to monitor tissue SO_2 in both large animal and human models of shock as noted earlier [10–15]. Our results here are similar to previously reported observations of decreases in peripheral tissue hemoglobin and tissue vascular saturation during shock, relative to baseline values. However, most previous reports have employed near infrared wavelengths (650-900 nm) for DRS measurements with source-detector separations of between 0.5 and 2 cm. However, we used DRS measurements in the visible spectrum (450-800 nm) with source-detector separation of 0.2 cm, thus rendering the sampling depth of DRS to be mostly confined to the upper 2 mm of the skin.

The DCS results were analyzed using two different flow models – one empirical and another based on the diffusion theory based model. Both techniques yielded nearly identical measures of blood flow and showed that blood flow in peripheral tissues was almost immediately impacted after hemorrhagic shock. The responses in the DRS-derived hemodynamic variables did not indicate as temporally high a sensitivity as DCS flow to shock. However, both these optical methods detected hemorrhagic shock much earlier than reflected by systemic indicators of MAP and CO. As hypothesized these results indicate compensatory vascular mechanisms in reaction to hemorrhage are were strongly present when optical measurements probed tissue volumes containing small vessels. Additionally, confining measurement to shallow depths could also minimize contamination of hemoglobin absorption by myoglobin absorbance, which would be especially important in hemorrhage since unlike hemoglobin, myoglobin oxygen does not change early during shock [34, 42].

5. Conclusions

Our findings validate the hypothesis that hemorrhagic shock due to soft tissue injury would be detectable in vascular responses of peripheral tissues measured using optical methods of DCS and DRS. Further, these techniques detected reduced cutaneous perfusion due to the body's compensatory shunt mechanism that seeks to preserve blood for vital organs. From optical measurements, perfusion was quantified using three complementary parameters: relative blood flow rates, total hemoglobin concentration, and tissue vascular oxygenation. In combination, these variables could provide a more robust and sensitive means to tracking and hemorrhage and resuscitation.

In summary, studies seeking to detect occult hemorrhage during the precompensatory phase in critically-ill or injured patients would benefit from employing such multimodal optical techniques for continuous noninvasive blood flow and hemoglobin monitoring.

Biomedical Optics EXPRESS

Acknowledgements

We wish to acknowledge support from the NIH (5R00CA140783-04) and facilities at RMD Inc during the data collection phase of these studies.

Disclosures

The authors declare that there are no conflicts of interest related to this article.